22kW EV Battery Charger Allowing Full Power Delivery in 3-Phase as well as 1-Phase Operation

P. Papamanolis,
F. Krismer,
J.W. Kolar

22 kW EV Battery Charger Allowing Full Power Delivery in 3-Phase as well as 1-Phase Operation

Panteleimon Papamanolis, Florian Krismer, and Johann W. Kolar

Power Electronic Systems Laboratory (PES)
ETH Zurich, Physikstrasse 3 / ETL / H23
8092 Zurich, Switzerland
Email: papamanolis@lem.ee.ethz.ch

Abstract—A new universal front-end PFC rectifier topology of a battery charger for Electric Vehicles (EVs) is proposed, which allows fast charging at rated and/or full power level in case of 1-phase (USA) as well as 3-phase (Europe) mains supply. For a conventional 3-phase PFC rectifier, only 1/3 of the rated power would be available in case of 1-phase operation. The new topology is based on a two-level six-switch (2LB6) 3-phase PFC rectifier, which is extended with a diode bridge-leg and additional windings of the Common-Mode (CM) chokes of the EMI filter. The focus of the paper is on the analysis of the generated CM and Differential Mode (DM) EMI noise for both operating modes, i.e., 1-phase and 3-phase operation, resulting in guidelines for EMI filter design. The suggested topology modifications are also applied to a three-level T-type (Vienna) PFC rectifier structure. The theoretical considerations are verified with simulations. Finally, a 22 kW prototype of the new universal PFC rectifier is designed using η-ρ Pareto optimization, targeting an efficiency of 98.4 %, a power density of 6.8 kW/dm³, i.e., a volume of 3.24 dm^3, and an EMI filter that ensures compliance with the CISPR class B EMI standard. Compared to a volume-optimized design of a conventional 3-phase topology of same power rating and efficiency, but limited 1-phase power transfer capability, the additional volume required for the proposed extension is less than 0.5 dm^3 (15 %) and therefore clearly justified considering the enabled universal applicability of the converter system.

I. INTRODUCTION

The increasing distribution of Electric Vehicles (EVs) results in a demand for universal front-end PFC rectifier topologies of EV chargers that facilitate full power operation in presence of 3-phase and 1-phase mains. For example, ≈ 20 kW of charging power should be available for connection to a 3-phase mains with line-to-line rms voltages of 400 V and a maximum phase current of 32 A in Europe [1], as well as 1-phase mains with 240 V rms voltage (three-wire split-phase system in the USA [2]) and a maximum current of 80 A (resulting in a maximum power of 19.2 kW).

Three individual 1-phase PFC AC/DC converter modules, as described e.g., in [3]–[5], can be interconnected to realize the universal front-end, which requires three individual stages comprising isolated DC/DC converters. Alternatively, according to **Fig. 1(a)**, a conventional 3-phase AC/DC converter readily enables 1-phase operation, cf. **Fig. 1(b)**, however, only for a reduced power of approximately 1/3 of the nominal 3-phase power, since the power components in each phase are only rated for the current occurring for nominal 3-phase operation [6], [7]. 1-phase operation at a total current of 80 A would be feasible with the configuration depicted in **Fig. 1(c)**, where phases a, b, and c are operated

in parallel and the split DC-link features a midpoint, O, for the connection of the return conductor and/or neutral line. In this configuration, however, the currents in the three windings of each Common Mode (CM) choke of the front-end EMI filter would be in-phase, which would lead to saturation of the magnetic core. Furthermore, each of the two capacitors of the split DC-link would need to alternately buffer energy during a half mains cycle and therefore would be subject to excessive current stress.

This paper, proposes modifications for the state-of-the-art two-level six-switch (2LB6) and the three-level T-type (3T2C) 3-phase PFC rectifier topologies, in order to enable operation at full power for both, 1-phase and 3-phase mains. The proposed topologies, together with a universal structure of the EMI filter, are described in **Section II**. The effectiveness of the EMI filter for 1-phase and 3-phase operation is analyzed in **Section III**. In **Section IV** the obtained findings are used for converter optimization and the results are verified by simulations. The finally designed universal 3-phase/1-phase PFC AC/DC converter features simulated efficiencies of 98.4 % and 97.8 % in 3-phase and 1-phase operation respectively, and a maximum power density of 6.8 kW/dm^3.

II. MODIFICATIONS FOR 1-PHASE OPERATION

Fig. 2 depicts the proposed modified 2LB6 PFC rectifier topology, employing a novel three-stage EMI filter structure, and **Tab. I** lists the main converter specifications along with the main component values. The 4-phase CM choke avoids core saturation in 1-phase operation, by magnetically coupling the input phase currents and the return current. Furthermore, a passive diode bridge-leg, instead of a direct connection to the DC-link midpoint, reduces the maximum RMS currents in the two DC-link capacitors from 44 A to 18 A. Finally, a relay contact is employed between the midpoints of the diode bridge-leg and the DC-link capacitors, which is needed to reduce CM noise in 1-phase operation, as discussed in Subsection II-B.

A. Structure of EMI Filter Stage

The EMI filter shown in Fig. 2 is realized using two different types of filter structures, denoted as type I and type II. **Figs. 3(a)-(d)** present alternatives of generic filter structures of type I, suitable for 3-phase and 1-phase operation. The proposed structures effectively attenuate the generated DM and CM noises for 3-phase as well as 1-phase
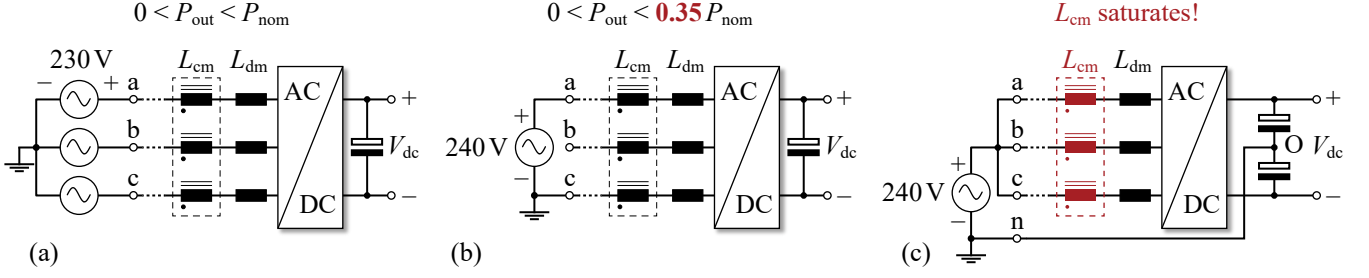
Fig. 1: Block diagrams of 3-phase AC/DC converters for different operating conditions: **(a)** operation from three-phase mains; **(b)** 1-phase operation between two phases [6]; **(c)** operation with phases a, b, and c in parallel. Configuration (c) is not feasible, due to saturation of the 3-phase CM choke.
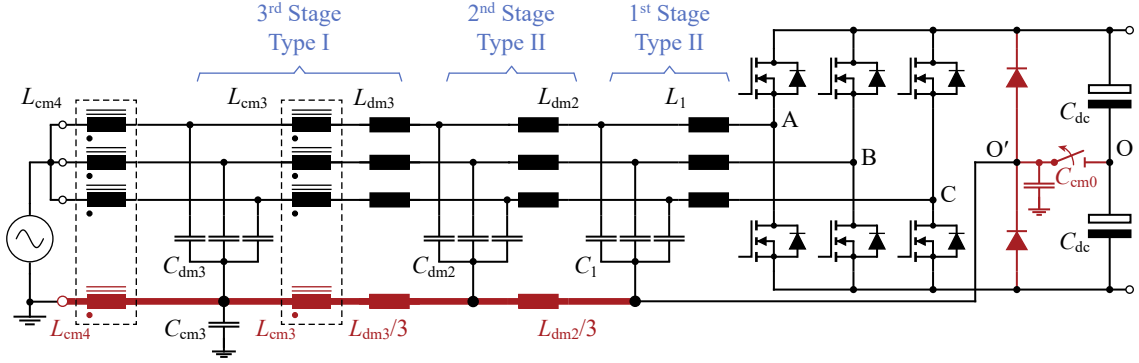

Fig. 2: Proposed two-level six-switch (2LB6) 3-phase AC/DC converter with three-stage EMI filter supplied by a 1-phase mains. Compared to a conventional 2LB6 rectifier topology, the additional components, highlighted with red color, allow full power delivery also for 1-phase operation, otherwise, the 1-phase rating would be limited to 1/3 of the rated 3-phase power (cf. Fig. 1(b)).

TABLE I: EV charger: specifications and design results.

Parameter	Description	Value
P_{nom}	Nominal power, 3-ph/1-ph	22 / 19.2 kW
$V_{ac,rms}$	Nominal input voltage, 3-ph/1-ph	230 / 240 V
$I_{ac,rms}$	Nominal input current, 3-ph/1-ph	32 / 26.67 A
f_{mains}	Nominal grid frequency, 3-ph/1-ph	50 / 60 Hz
V_{dc}	Nominal output voltage	750 V
f_s	Switching frequency	48 kHz
L_1	Inductance of 1st filter stage	150 µH
C_1	Capacitance of 1st filter stage	10 µF
L_{dm2}	DM inductance of 2nd filter stage	5 µH
C_{dm2}	DM capacitance of 2nd filter stage	3.3 µF
L_{cm2}	CM inductance of 2nd filter stage	1.5 mH
C_{cm2}	CM capacitance of 2nd filter stage	20 nF
L_{dm3}	DM inductance of 3rd filter stage	3 µH
C_{dm3}	DM capacitance of 3rd filter stage	2.2 µF
L_{cm3}	CM inductance of 3rd filter stage	750 µH
C_{cm0}	CM capacitor of the DC-side	15 nF
C_{dc}	Capacitor of split DC-link	2.7 mF

mains operation (cf. Fig. 2). The main trade-off between the four alternatives is the number of the filtering components and the symmetry of their arrangement, since structural asymmetries can cause mixed-mode noise emissions [8]. In all four structures, a 4-phase CM choke is employed and a low impedance return path for the CM noise of the switching stage is provided through the Protective Earth (PE) and C_{cm0} (cf. Fig. 2). The considered converter employs the

structure depicted in Fig. 3(d), since it has the least amount of capacitors and therefore features lowest volume.

Figs. 3(e), (f) depict potential realizations of the 4-phase CM choke, using a toroidal core. The 4th winding is split into the parts n_I, n_{II}, and n_{III}, that are distributed over the circumference of the toroidal core and connected in parallel or in series, in order to maintain symmetry and achieve low parasitic capacitances. The 4th winding is subject to the full phase current in 1-phase operation. Hence, its cross section is three times larger than those of the wires of the three phases (cf. Fig. 3(f)). This cross section ratio ensures equal distribution of LF winding losses and therefore better thermal performance. From the two alternative realizations, the structure of Fig. 3(f) achieves increased copper fill factor (i.e., decreased LF winding losses) and higher coupling factor and is used for the considered PFC rectifiers.

According to [9], in order to effectively reduce High Frequency (HF) voltage components that occur between the midpoint, O, and the earth potential, the artificial star-point, formed by the three DM filter capacitors, could be directly connected back to the midpoint, O. However, in this case the CM chokes of the structures shown in Figs. 3(a)-(d) would be ineffective, since the generated HF CM noise component would prefer the highlighted path in **Fig. 4(a)**, instead of the path through L_{cm} and C_{cm}, where the only component of considerable impedance would be the stray inductance of the CM choke. Therefore, in order to preserve
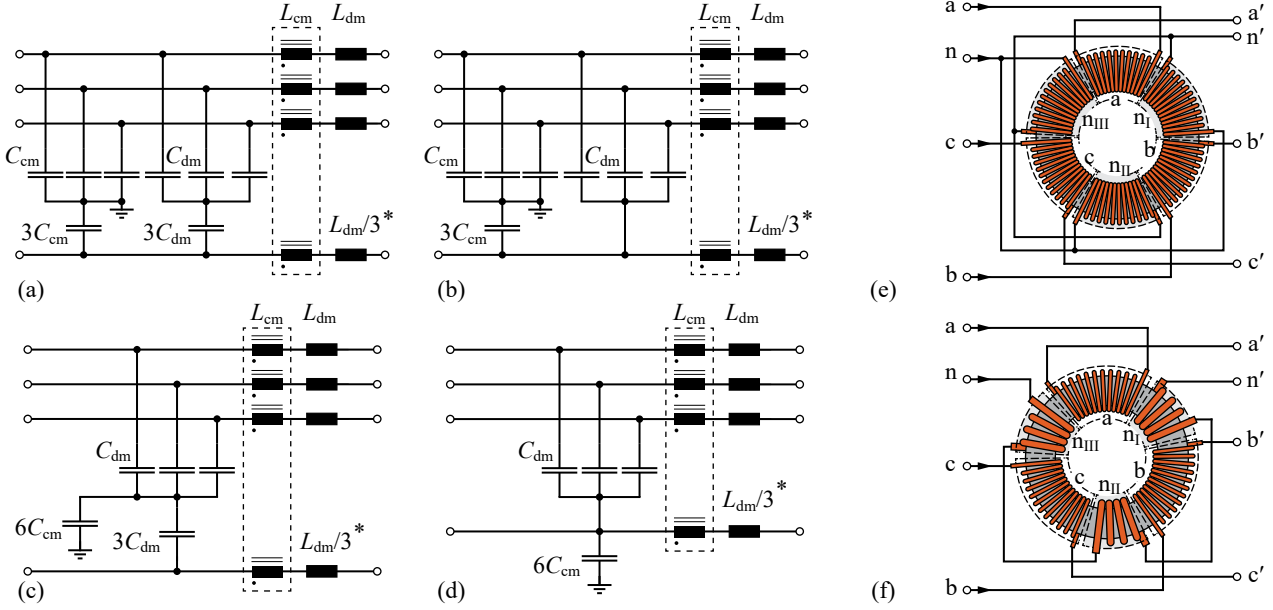
Fig. 3: (a)-(d) Proposed structures for a single stage of the EMI filter that are effective in 1-phase as well as 3-phase operations (type I). $L_{dm}/3$ (marked with an *) is included for symmetry reasons and may be omitted. **(e)**, **(f)** Schematic drawings of two different constructions of the 4-phase CM choke, using a toroidal core and 12 turns per phase: the three windings of the neutral line can be connected in parallel **(e)** or in series **(f)**, to form the 4th phase of the CM chokes of the 2nd and 3rd EMI filter stage (cf. Fig. 2).
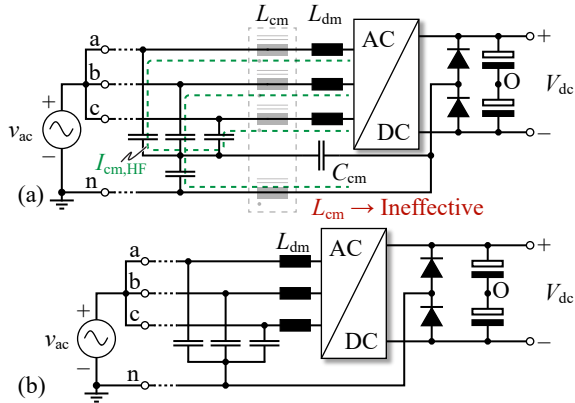

Fig. 4: (a) Path of the HF CM current in case of type I filter structures and CM feedback by means of C_{cm}; $i_{cm,HF}$ prefers the path through the 4th winding of the CM choke, which renders L_{cm} and C_{cm} ineffective. **(b)** alternative solution for the same case (type II, cf. 1st EMI filter stage in Fig. 2).

effective operation of the EMI filter in both operating modes, a modified filter structure without CM choke, depicted in **Fig. 4(b)**, is proposed (type II). The proposed PFC rectifiers employ both types of filter structures, with type II being directly connected to the converter switching stage (cf. Fig. 2).

B. CM capacitor on the DC side

For the sake of symmetry, a CM capacitor on the DC-side of a conventional 3-phase converter would either be shared between DC+ and DC- or would be directly connected to the midpoint of the DC-link (C_{cm0} of Fig. 2 for the relay switch being closed). In both cases, the effect on the attenuation would be ideally identical, since, from a HF perspective, the capacitors of the DC-link (commonly in the µF/mF range) can be considered to approximately represent short-circuits at the frequencies relevant for conducted EMI. The capacitor C_{cm0} features the benefits listed below:

- Provision of a low-impedance/controlled return path for the HF CM components through PE.
- Decrease of the DC-side EMI CM noise, i.e., between O and PE, and the AC-side EMI CM noise, which is explained in Section III.

However, in 1-phase operation, C_{cm0} causes an increase of the CM EMI noise at the AC and the DC sides. This is explained based on **Fig. 5(a)**, which depicts the 1-phase equivalent of the suggested structure, together with the 1st stage of the EMI filter and an additional CM inductor. Based on the assumption that the neutral line of the grid and PE are at the same potential, every zero crossing of the LF current, which results in a commutation between the two diodes, leads to an abrupt voltage step equal to V_{dc} across C_{cm0} and a resonant current through C_{cm0} and L_{cm}. **Fig. 5(b)** depicts the currents through the LISN, in case of the complete EMI filter of Fig. 2, which oscillate at approximately 30 kHz and are increasing the noise floor by 40 dB (in the real application, the generated noise will be limited by the finite dv/dt of the voltage transitions). It should be noted, that for a split-phase power system, where the earth potential is between the two potentials of the two mains phases, the same superimposed voltage step is present across C_{cm0}.

In order to overcome the aforementioned drawback, C_{cm0} could be connected directly to the switching node of the
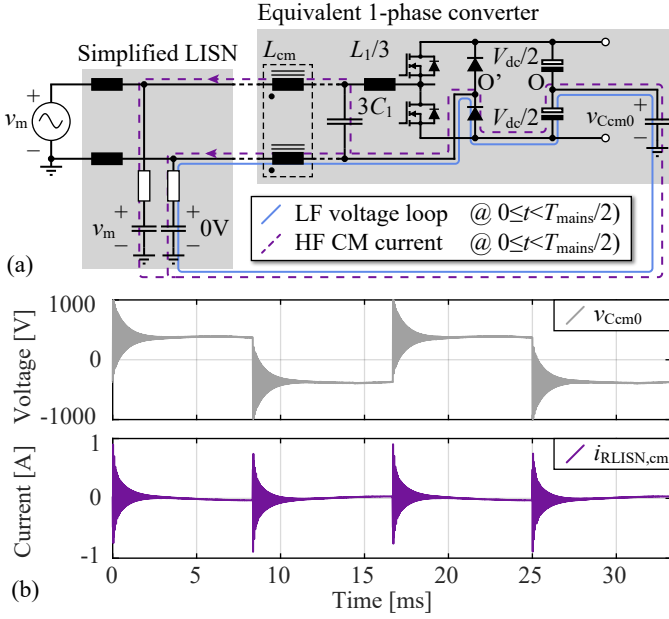
Fig. 5: (a) 1-phase equivalent circuit of Fig. 2 (for the sake of simplicity, only the 1$^{\text{st}}$ stage of the EMI filter and a CM inductor are depicted). The noise emission path (enclosing the neutral line, the PE and C_{cm0}) and the HF resonance path of the CM current (through C_{cm0} and R_{LISN}) are highlighted; **(b)** Voltage waveform of the voltage across capacitor C_{cm0} and CM current waveform through the LISN for two mains periods at 60 Hz.

diode half-bridge, O'. In this case, the voltage across C_{cm0} would be constant. However, such connection would render C_{cm0} ineffective in 3-phase operation, since the diodes then do not conduct. To make C_{cm0} always effective, a relay contact is inserted between the midpoints, O and O', which is closed in 3-phase operation and remains open for 1-phase operation.

C. Extension to Three-Level Converter

The above-mentioned extensions (including the LF diode bridge-leg) can be applied to any conventional multilevel 3-phase system, that can be implemented without the DC-link midpoint (e.g., a Flying Capacitor Converter). However, converters with inherent utilization of the midpoint (e.g., the Vienna Rectifier and/or a T-type converter) cannot be extended by a diode bridge-leg according to Fig. 2. Still, 1-phase operation is possible by direct connection of the neutral line to the DC-link midpoint, O, which, however, would result in excessive RMS currents in the DC-link capacitors and would require large DC-link capacitances (approximately 8 mF per half DC-link, for the specifications according to Tab. I). In order to overcome this disadvantage, the following modifications are applied to the well-known T-type converter structure of **Fig. 6**:

- A LF diode bridge-leg is added (similar to the 2LB6 converter extension).
- A relay circuit for series/parallel reconfiguration of the DC-link capacitors and the subsequent DC/DC converters is provided.

Furthermore, the operating mode of the converter is selected dependent on the type of mains supply:

- Three-level operation for 3-phase mains connection ($V_{\text{dc}} = 750\,\text{V}$ - middle leg enabled).
- Two-level operation for 1-phase AC input ($V_{\text{dc}} = 375\,\text{V}$ - middle leg disabled).

For the proposed system, the voltage-time product applied to the magnetic components of the EMI filter is similar in both operating modes and the LF rms current of each capacitor of the DC-link in 1-phase operation is equal to the one of the 2LB6 converter.

III. GENERATED EMI NOISE AND FILTERING

This Section provides individual analyses for the 3-phase and the 1-phase operations, to gain a detailed understanding of the generated noise components. According to the CISPR 16 regulations, measurements of the generated EMI noise need to be conducted with a test receiver, using average or Quasi-Peak (QP) detectors, with the noise level expressed in dBμV. The circuit models of the detectors are nonlinear systems that include diodes and, as a result, an analytic calculation of the generated noise is hardly possible. Therefore, [10] proposes an approximation, that neglects correlations between individual frequency components. For the defined receiver bandwidth (RBW) of 9 kHz (according to CISPR 16 regulations), the generated noise is determined using:

$$\max_{\text{noise}}(f) = 20\log_{10}\left(\frac{1}{1\mu V}\sum_{\xi=f-\frac{\text{RBW}}{2}}^{\xi=f+\frac{\text{RBW}}{2}} V_{\text{meas}}(\xi)\right). \quad (1)$$

This concept, i.e., (1), will be employed in the following for both, i.e., the DM and the CM component, of the EMI noise.

A. Conducted EMI for 3-Phase Operation

Fig. 7(a) depicts the HF EMI model corresponding to the topology shown in Fig. 2 for closed relay contact. The EMI noise source is modeled with three DM sources and one CM source. Furthermore, Fig. 7(a) considers three parasitic capacitors ($C_{\text{parasitic}}$)[1], because these capacitors are found to substantially deteriorate the effective attenuation of the CM EMI filter.

The waveforms of the DM and CM voltages are obtained with

$$v_{\text{dm},i} = v_{i\text{O}} - v_{\text{cm}}, \quad \forall\ i \in \{\text{A,B,C}\}. \quad (2)$$

In Fig. 7(a) a path of a HF DM EMI noise current is highlighted in red color, and the achieved attenuation per stage, k, in dB is equal to:

$$\text{Att}_{k,\text{dB}} = 20\log_{10}\left(\omega^2 C_k L_k\right), \quad (3)$$

for frequencies much greater than the crossover frequency.

---

[1]Due to the grounded heatsink of the semiconductors, the value of $C_{\text{parasitic}}$ can be approximated by the total surface of the metallic backplates of the low-side MOSFETs, the permittivity of the interface material, and the distances between the metallic backplates and the heatsink surface, which for two parallel MOSFETs (TO-247 packages), leads to $3C_{\text{parasitic}} = 225\,\text{pF}$.
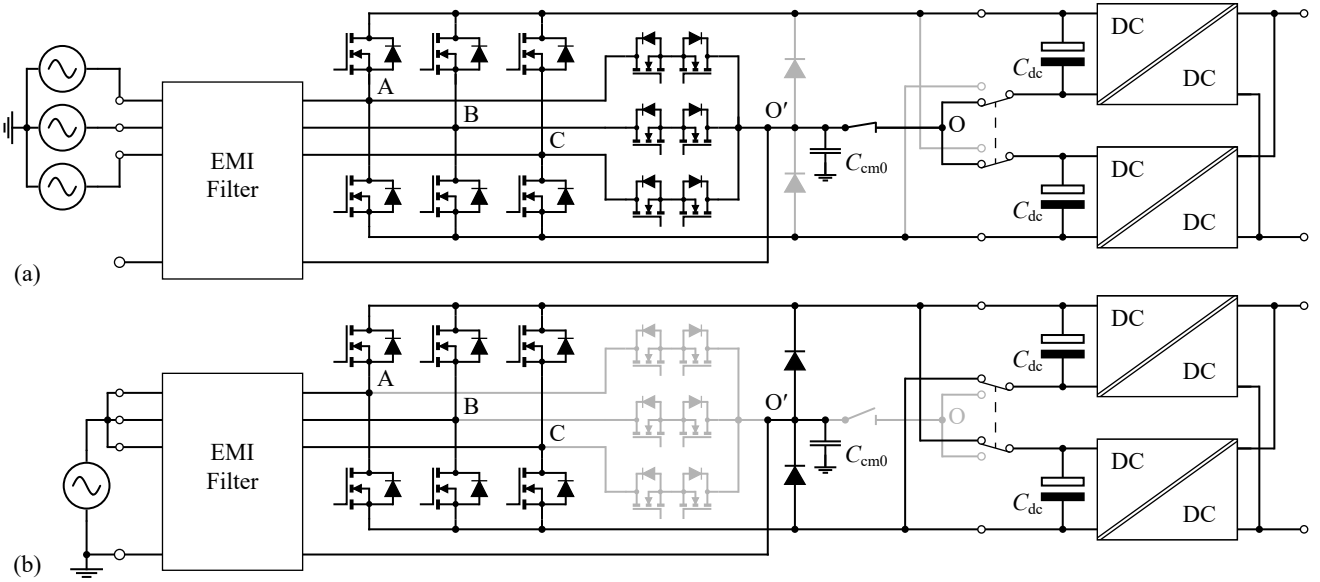
Fig. 6: Application of the proposed extensions to the T-type AC/DC rectifier: **(a)** 3-phase operation with a DC-link voltage of 750V; **(b)** 1-phase operation with a DC-link voltage of 375V.

Without consideration of $C_{\text{parasitic}}$, the equivalent circuit for EMI CM noise is depicted in **Fig. 7(b)**. Assuming initially that C_{cm0} is equal to 0, only the stray inductance of L_{cm3} is effective, due to the magnetically coupled return currents, however, very high attenuation of the generated CM noise is still achieved, due to the DM filter components, C_{cm3}, and L_{cm4}.

Installation of C_{cm0} lowers the attenuation, by reason of a parallel current path for CM EMI noise (highlighted in Fig. 7(b)), however, still it is found that with the EMI filter component values of Tab. I, v_{cm} is attenuated to values well below the EMI limits of CISPR 16.

With $C_{\text{parasitic}}$ being considered, the equivalent circuit of **Fig. 7(c)** results, which enables the derivation of a simplified CM EMI model in the style of [11]. In this context, in a first step, $L_1/3$ is replaced by an open circuit, $3C_1$ by a short-circuit and the CM noise source by its Thévenin equivalent source, cf. **Fig. 7(d)**, where C_{cm0} features a first reduction of the CM noise voltage. Since the HF impedance of C_{eq} is found to be negligible, compared to the subsequent magnetic components, Fig. 7(d) can be further simplified to the structure depicted in **Fig. 7(e)**, revealing the effectiveness of L_{cm3}. The generated noise, due to $C_{\text{parasitic}}$, is affecting both, the DC and the AC sides of the converter. Increased value of C_{cm0} would improve the attenuation, due to the voltage division, nevertheless its value is limited by the touch current in 1-phase operation.

The analytic considerations have been fully verified by means of simulations and, for the 2LB6 PFC rectifier designed in Sec. IV, with the component values of Tab. I, the CM noise by reason of $C_{\text{parasitic}}$ has been found to exceed the CM noise without $C_{\text{parasitic}}$, determined according to Fig. 7(b), by +35dB. For this reason, Fig. 7(e) is considered for the design of the CM filter.

B. Conducted EMI of 1-Phase Operation

In 1-phase operation, interleaved modulation of the three bridges (i.e., A, B, C) is used, because it decreases the HF RMS currents in the DC-link capacitors from 42A (without interleaving) to 12A, and it decreases the required attenuation of the CM filter in 1-phase operation, which is further explained in Sec. III-C. A simple proportional controller is required to ensure equal distribution of the DM LF currents between the three parallel phases.

The DM equivalent circuit is depicted in **Fig. 8(a)**, where only the frequency multiples equal to $(3k+3)f_{\text{s}}, k \in \mathbb{N}_0$, are common for all three phases and appear in the LISN. The remaining HF harmonics circulate between the three phases and, in case of an ideally symmetric filter, do not lead to significant voltages at the LISN.

Without consideration of $C_{\text{parasitic}}$, the equivalent circuit for the filtering of the harmonics with ordinal numbers of $(3k+3), k \in \mathbb{N}_0$, depicted in **Fig. 8(b)**, is similar to Fig. 7(b), except that the neutral line is also connected to the LISN. As a result, only the DM filter components and the stray inductances of L_{cm3} and L_{cm4} are effective and the parallel path through C_{cm0} and C_{cm3} is ineffective, since, in the given system, $Z_{\text{Lcm4},\sigma} \ll Z_{\text{Ccm3}}$ is valid up to high frequencies ($> 5\,\text{MHz}$).

In 1-phase operation, the LF switching of the mains rectifier diodes and $v_{\text{dm},(3k+3)}, k \in \mathbb{N}_0$, are causing CM noise. The CM noise of the rectifier diodes is resolved by correct placement of C_{cm0}. Thus, the only relevant CM noise is caused by $v_{\text{dm},(3k+3)}, k \in \mathbb{N}_0$, and by reason of $C_{\text{parasitic}} > 0$. The derivation of the effective EMI filter is identical to that of 3-phase operation presented in Sec. III-A, cf. **Fig. 8(c)-(e)**, with a small difference in the last stage, where the value of $R_{\text{LISN}}/2$ is used instead of $R_{\text{LISN}}/3$.

C. Basic Design Guideline for the EMI Filter

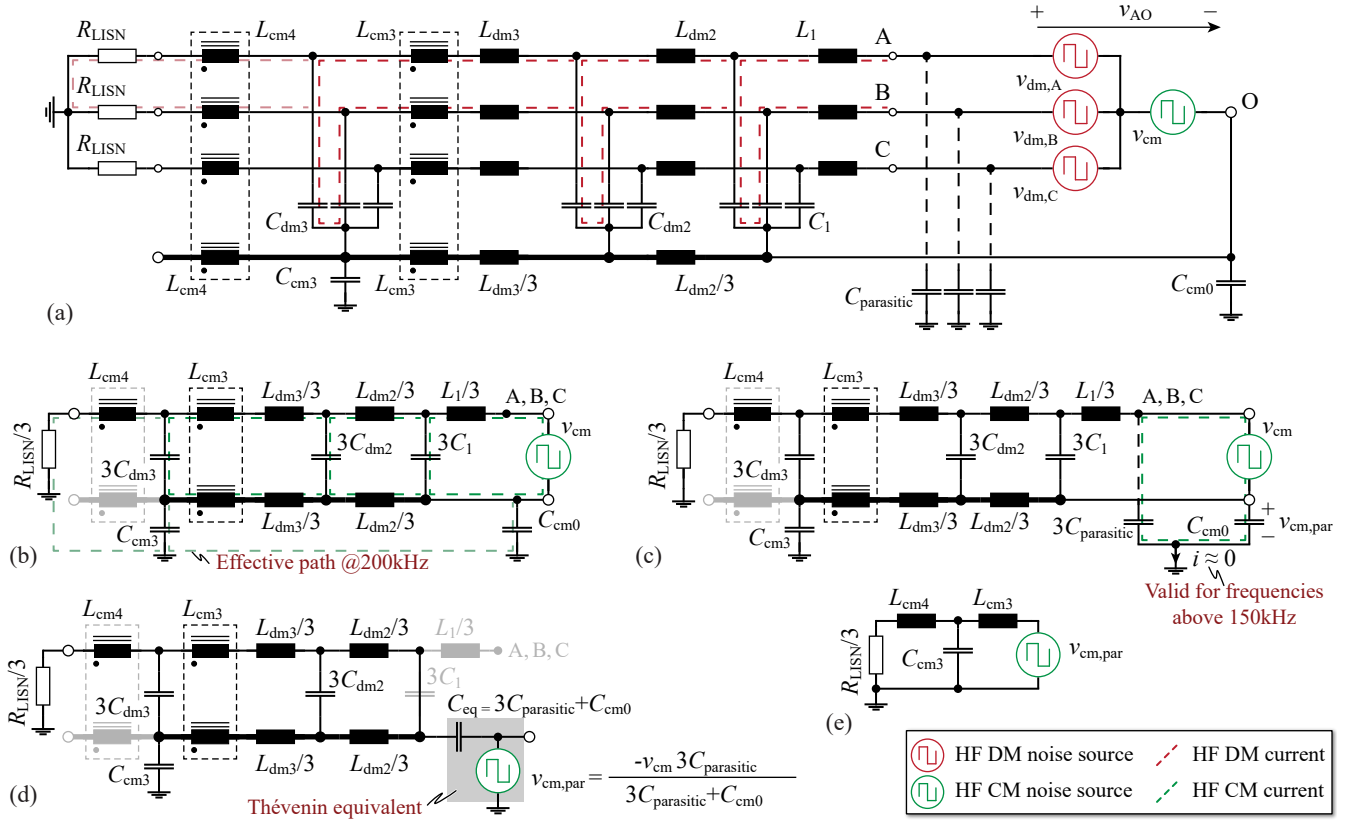The analyzed converter system incorporates three important sources of conducted EMI, i.e., $v_{\text{dm},\{A, B, C\}}$ and v_{cm} of

Fig. 7: (a) HF equivalent circuit of the 2LB6 converter shown in Fig. 2, for 3-phase operation; **(b)** CM equivalent circuit if the parasitic capacitances $C_{\text{parasitic}}$, between the switching nodes and PE (e.g., due to grounded heatsinks), is neglected; **(c)-(e)** CM equivalent circuit for $C_{\text{parasitic}} > 0$.

TABLE II: EMI generated noise.

Source	Operation	CISPR Freq. [kHz]	Max Noise [dBµV]
$v_{\text{dm,i}}$	3-phase	192	162
v_{cm}	3-phase	192	153.6
$v_{\text{cm,par}}$	3-phase	192	118
$v_{\text{dm,(3k+3)}}$	1-phase	288	162.3
$v_{\text{cm,par}}$	1-phase	288	126

Fig. 7 and $v_{\text{dm,(3k+3)}}$ of Fig. 8. The calculated noise voltages for each source are presented in **Tab. II** and verified with simulations.

For the investigated system it was found sufficient to design the DM components of the EMI filter, such that the CISPR limitation (plus margin of 10 dB) is fulfilled in case of 3-phase operation (cf. Fig. 7(a)), and to design the CM part of the filter for the equivalent circuit of Fig. 7(e). With this, the other noise sources are attenuated with margins greater than 30 dB, except for the CM noise through $C_{\text{parasitic}}$ in 1-phase operation, where the margin is 10 dB at 288 kHz. However, this result is only achieved through interleaving; without interleaving, the CISPR limit would be violated by 1 dB at 192 kHz. A benefit is only attained if the ordinal number of the first harmonic that enters the CISPR regulated frequency range belongs to $\{3k+1, 3k+2\}$, $k \in \mathbb{N}_0$, which is valid for $f_s = 48$ kHz.

IV. CONVERTER DESIGN AND VERIFICATION

The design of a hardware prototype of the proposed AC/DC converter for a 22 kW EV charger is performed based on an η-ρ Pareto optimization [12]–[14], which employs coupled electro-thermal and magneto-thermal component models and takes different switching frequencies (between 24 kHz and 144 kHz), inductor current ripple values (relative peak-to-peak values between 10 % and 50 %), and magnetic core materials (ferrite, iron powder) into account. The selected optimized design achieves a simulated efficiency of 98.4 % in 3-phase operation and 97.8 % in 1-phase operation, and a maximum power density of 6.8 kW/dm³ for the complete converter system; a virtual 3D model is depicted in **Fig. 9**. The efficiency drop in 1-phase operation is mainly due to the additional conduction losses of the diode bridge-leg, which are equal to 93 W. Tab. I lists main specifications and corresponding design results. Two parallel C2M0040120D SiC MOSFETs (Wolfspeed/CREE) are employed for realizing each switch, and three parallel Si diodes (VS-80APRF10 series, Vishay) for each LF diode, which are of low-cost and feature a forward voltage of 1 V at an average current of 24 A. Iron-powder KoolMu material is used for the boost inductors and film capacitors (X and Y rated) for the capacitors of the EMI filter. Aluminum electrolytic capacitors realize an effective DC-link capacitance of $C_{\text{dc}}/2 = 1.35$ mF; the total boxed volume of all DC-link capacitors is 0.5 dm³.

The considered system uses the same DC-link voltage (750 V) for operation with 1- and 3-phase mains. With this
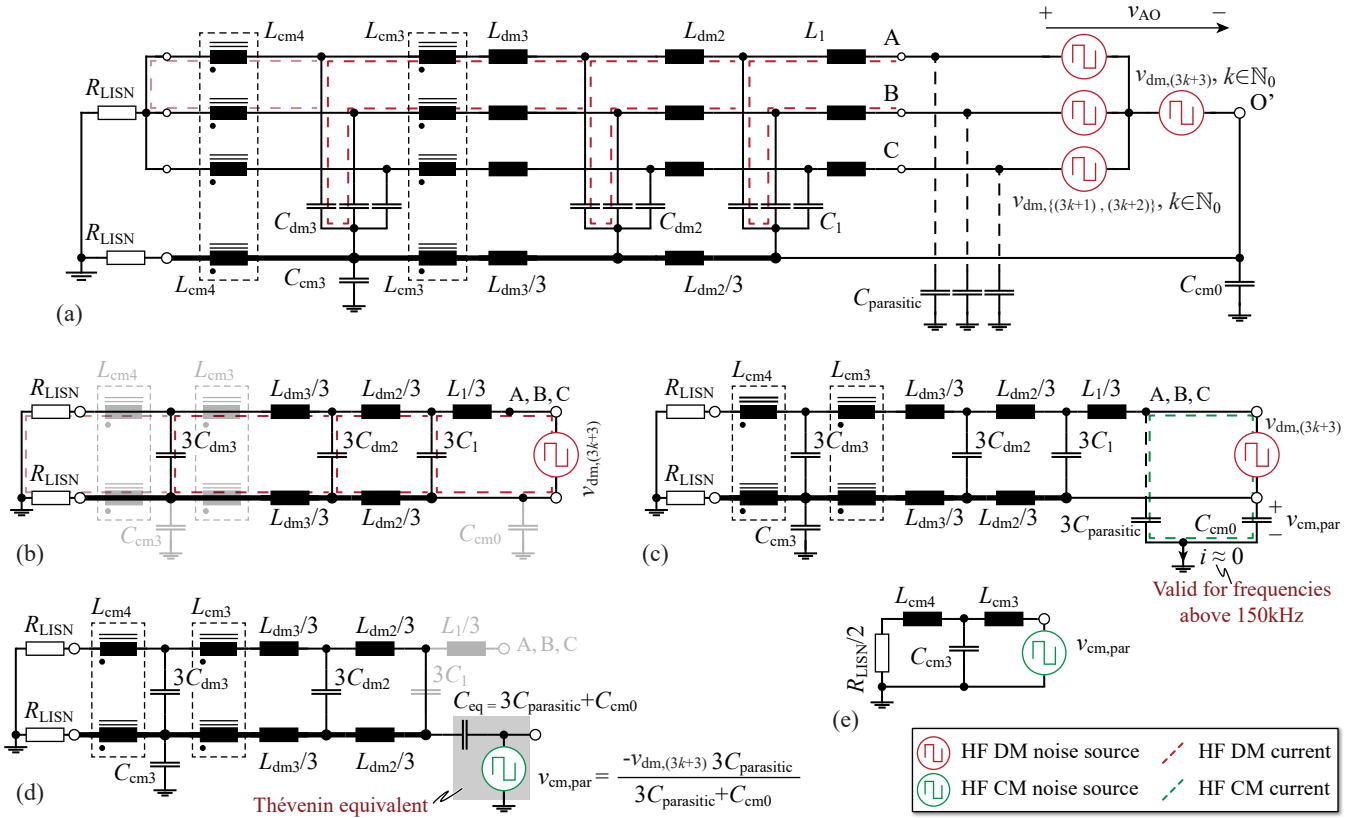
Fig. 8: **(a)** HF equivalent circuit of the 2LB6 converter shown in Fig. 2, for 1-phase operation; the conduction paths of the HF current harmonics at $(3k+1)f_s$ and $(3k+2)f_s, k \in \mathbb{N}_0$, are highlighted; **(b)** DM 1-phase equivalent circuit considering the HF current harmonics at $(3k+3)f_s, k \in \mathbb{N}_0$; **(c)-(e)** CM equivalent circuit considering $C_{parasitic} > 0$.
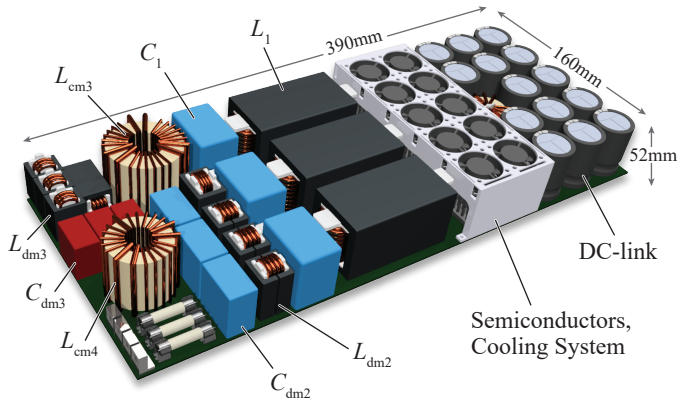

Fig. 9: 3D illustration of the designed universal 22 kW 2LB6 rectifier and/or EV charger front-end. The converter achieves a maximum power density of 6.8 kW/dm³ and an estimated efficiency of 98.4 % in 3-phase operation and 97.8 % in 1-phase operation.

operation, the switches' rms currents are 20 A for 1-phase operation at 19.2 kW and 23 A for 3-phase operation at 22 kW. However, the losses in each boost inductor, L_1, increase from 22 W in case of 3-phase operation to 29 W in 1-phase operation, due to different current ripples.

Figs. 10(a), **(b)** depict simulated waveforms for 3-phase and 1-phase operation, respectively. According to these results, the DC-link voltage shows a peak-to-peak voltage ripple of 50 V in 1-phase operation, due to the power pulsation with twice the mains frequency.[2] **Figs. 10(c)**, **(d)** depict simulated spectra of conducted EMI, which verify the validity of the analytic considerations presented in Sec. III ('max. noise' in Figs. 10(c) and 10(d) denotes the maximum estimation according to (1)). In addition, the absence of frequency multiples equal to $\{3k+1, 3k+2\}, k \in \mathbb{N}_0$, in 1-phase operation is depicted.

V. CONCLUSION

The proposed universal 3-phase/1-phase front-end AC/DC converter of a 22 kW EV charger facilitates fast charging in countries providing 3-phase 400 V/32 A or 1-phase 240 V/80 A mains connections. For a two-level six-switch (2LB6) converter topology this is achieved with a modified power stage, that provides a dedicated return conductor for 1-phase operation and a novel EMI filter structure that features 4-phase Common Mode (CM) chokes, which do not saturate in case of 3-phase or 1-phase operation. The suggested modifications are further applied to a three-level T-type converter. The conducted EMI noise is analyzed and the effectiveness of each filter component is discussed for both operating modes. In addition, general EMI filter design guidelines are presented. The discussed solution is

---

[2]In the final EV charger application, the realized AC/DC converter will be connected to a DC–DC converter stage with galvanic isolation, which continuously adapts to the changing DC-link voltage and provides a constant output voltage [15].
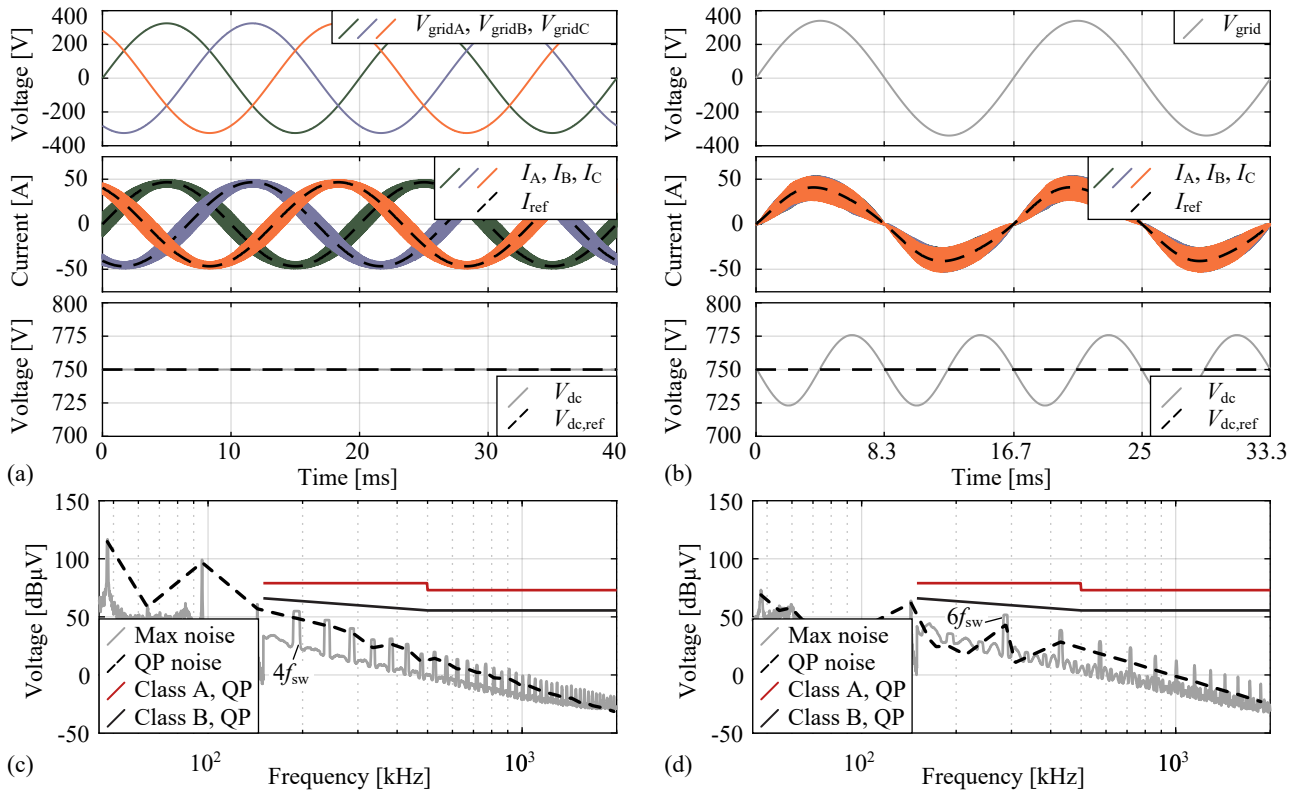
Fig. 10: Simulation results for the proposed 22 kW EV charger and/or AC/DC converter specified in **Tab. I**. Main waveforms and conducted EMI: **(a)**, **(c)** for 3-phase and **(b)**, **(d)** for 1-phase operation.

validated by means of circuit simulations and a prototype is designed based on η-ρ Pareto optimization. The resulting system achieves a power density of 6.8 kW/dm^3 and a simulated efficiency of 98.4 % in 3-phase and 97.8 % in 1-phase operation. Compared to an optimized conventional 2LB6 3-phase PFC rectifier with the same efficiency and rated power, which would be limited to $\approx$ 7 kW for 1-phase mains operation, the volume increases from 2.8 dm^3 to 3.3 dm^3. In addition, the proposed solution still features low complexity and the modifications are of low cost.

REFERENCES

[1] "Plugs, socket-outlets, vehicle connectors and vehicle inlets – conductive charging of electric vehicles," *IEC 62196*.

[2] "SAE surface vehicle recommended practice J1772, SAE electric vehicle conductive charge coupler," *SAE J1772*.

[3] "RFM - Power Tablet™ 3-Phase AC to 48V converter," *http://www.vicorpower.com/industries-computing/RFM.html*, (accessed October 30, 2018).

[4] J. Schmenger, S. Endres, S. Zeltner, and M. März, "A 22 kW on-board charger for automotive applications based on a modular design," in *Proc. of the IEEE Conf. on Energy Conversion (CENCON)*, Oct. 2014.

[5] J. Lu, K. Bai, A. R. Taylor, G. Liu, A. Brown, P. M. Johnson, and M. McAmmond, "A modular-designed three-phase high-efficiency high-power-density EV battery charger using dual/triple-phase-shift control," *IEEE Trans. on Power Electron.*, vol. 33, no. 9, pp. 8091–8100, Sept. 2018.

[6] BRUSA Elektronik AG, "NLG664 - On Board Fast Charger," in *NLG664 Datasheet*, May 2018.

[7] K. Stengert, "On-board 22 kW fast charger 'NLG6'," in *Proc. of the World Electric Vehicle Symposium and Exhibition (EVS27)*, Nov. 2013.

[8] K. Raggl, T. Nussbaumer, and J. W. Kolar, "Guideline for a simplified differential-mode EMI filter design," *IEEE Trans. on Ind. Electron.*, vol. 57, no. 3, pp. 1031–1040, March 2010.

[9] J. W. Kolar, U. Drofenik, J. Miniböck, and H. Ertl, "A new concept for minimizing high-frequency common-mode EMI of three-phase PWM rectifier systems keeping high utilization of the output voltage," in *Proc. of the IEEE Applied Power Electronics Conf. and Expo. (APEC)*, vol. 1, Feb. 2000, pp. 519–527.

[10] M. L. Heldwein, "EMC filtering of three-phase PWM converters," *Ph.D. dissertation*, ETH Zurich, 2008.

[11] H. Ye, Z. Yang, J. Dai, C. Yan, X. Xin, and J. Ying, "Common mode noise modeling and analysis of dual boost PFC circuit," in *Proc. of the IEEE Int. Telecom. Energy Conf. (INTELEC)*, Sep. 2004, pp. 575–582.

[12] J. W. Kolar, J. Biela, S. Waffler, T. Friedli, and U. Badstuebner, "Performance trends and limitations of power electronic systems," in *Proc. of the International Conf. on Integrated Power Electronics Systems (CIPS)*, March 2010.

[13] R. Burkart, "Advanced modeling and multi-objective optimization of power electronic converter systems," *Ph.D. dissertation, ETH Zurich*, 2016.

[14] P. Papamanolis, F. Krismer, and J. W. Kolar, "Minimum loss operation of high-frequency inductors," in *Proc. of the IEEE Applied Power Electronics Conf. and Expo. (APEC)*, March 2018, pp. 1756–1763.

[15] Infineon Technologies AG, "Comprehensive solutions for fast EV charging design," Jan. 2019.

[16] M. Uno, "Series-parallel reconfiguration technique for supercapacitor energy storage systems," in *Proc. of the IEEE TENCON*, Jan. 2009.